Rapid Communications

Timing angular momentum transfer for parity-unfavored transitions in multiphoton ionization

Meng Han,[1] Hao Liang,[1] Peipei Ge,[1] Yiqi Fang,[1] Zhenning Guo,[1] Xiaoyang Yu,[1] Yongkai Deng,[1] Liang-You Peng,[1,2,4] Qihuang Gong,[1,2,4] and Yunquan Liu[1,2,3,4,*]

[1]*State Key Laboratory for Mesoscopic Physics, Frontiers Science Center for Nano-Optoelectronics, Collaborative Innovation Center of Quantum Matter, School of Physics, Peking University, Beijing 100871, China*

[2]*Collaborative Innovation Center of Extreme Optics, Shanxi University, Taiyuan, Shanxi 030006, China*

[3]*Center for Applied Physics and Technology, HEDPS, Peking University, Beijing 100871, China*

[4]*Beijing Academy of Quantum Information Sciences, Beijing 100193, China*

(Received 24 June 2020; revised 8 November 2020; accepted 13 November 2020; published 3 December 2020)

When a bound electron is photoionized from an atom or molecule, the remaining multielectron ion with excess internal energy will relax towards lower-energy states. The subsequent transverse angular momentum transfer between the parent ion and the ejected electron can lead to an electron parity-unfavored transition. Here we perform a self-calibrated timing experiment to measure the time delay of the angular momentum transfer of parity-unfavored transitions during the multiphoton ionization. We use a strong linearly polarized 400-nm light field to trigger a parity-unfavored transition in the channel of the spin-orbit excited ionic state of krypton atoms and then selectively probe the phases of the electron wave functions with different magnetic quantum numbers with a weak parallelly (orthogonally) polarized 800-nm light field. The parallel and orthogonal probes serve as the start and the stop of a stopwatch, respectively. Hence, this allows us to access the characteristic time of such an ultrafast intra-atom multielectron process.

DOI: 10.1103/PhysRevA.102.061101

Photoionization of atoms is one of basic electron dynamical processes where the electrons can be removed from atoms by absorbing one or more photons, generally leaving behind a multielectron ion. The angular momentum transfer among electron, photon, and ion dictates that photoionization can be classified as parity-favored or parity-unfavored transitions [1–4]. The parity-favored transition is well understood by the selection rule of the magnetic quantum number m (i.e., $\Delta m = 0, \pm 1$ by absorbing each photon) within the single-active-electron approximation. In this case, the ejected electron totally absorbs the spin angular momenta of photons and converts them to its own orbital angular momentum, whereas the ion is viewed as a spectator. By contrast, when the electron-ion correlations come into play, the parity-unfavored transition will occur [5–7] in which the ion exchanges transverse angular momenta (characterized by the magnetic quantum number) with the ejected electron when relaxing to lower states [5,6]. As a result, the photoelectron emits perpendicularly with respect to the light polarization. Previous studies [1–9] on the parity-unfavored transition mostly focus on the peculiar photoelectron angular distribution. As a fundamental multielectron process, the timescale of the parity-unfavored transition is yet unclear. Time-resolving correlated multielectron dynamics is one of central topics in both ultrafast science [10] and condensed-matter physics [11] nowadays.

Recent advances [12–14] in attosecond metrology have opened the door to trace intra-atomic electron dynamics on the fastest measurable timescale, providing a new perspective of the fundamental photophysical and photochemical processes in the time domain. Attosecond time delays have been observed in the photoionization of atoms [15,16], molecules [17], and solids [18]. Generally, the time delays are measured with the attosecond streaking camera [12,19] or the reconstruction of attosecond beating by interference of two-photon transition (RABBIT) technique [13,20]. Recently, owing to the flexibility of controlling the polarization of visible lights, a variation of the RABBIT with a fundamental light field and its second harmonic has been introduced to temporally resolve the electron dynamical processes triggered by visible lights [21–24]. However, for most of the attosecond timing experiments only the relative time delay (or phase shift) of the process of interest with respect to other channels is measured. The absolute duration time of an ultrafast process can hardly be acquired since it is difficult to determine the start time and the end time of a process which occurs within a light cycle.

In this Rapid Communication, we present a self-calibrated timing experiment to measure the absolute duration time of the angular momentum transfer for a parity-unfavored transition in krypton atoms with two-color (400- + 800-nm) light fields. In the strong linearly polarized 400-nm field, the parity-unfavored transition occurs in the channel of the spin-orbit excited ionic state with the angular quantum number $J_i = 1/2$. In the parity-unfavored transition the electron angular momentum varies from d_0 ($l = 2$, $m = 0$) to d_2 ($l = 2$, $m = 2$). A weak parallel (or orthogonal) linearly polarized 800-nm light field is used to probe the phase of the electron wave packet populated in the d_0 (or d_2) state through a RABBIT-

*Yunquan.liu@pku.edu.cn

type scheme, analogous to the start (or stop) of a stopwatch. In whatever the parallel two-color (PTC) or the orthogonal two-color (OTC) light fields, the retrieved phase from the time-resolved sideband spectrum is calibrated with the reference of the ground ionic state ($J_i = 3/2$), based on the fact that the relative delay between the two ionic states of krypton can be inherently negligible (less than 8 as) [25]. Using the self-calibrated stopwatch, we measured the characteristic time of -255 ± 81 as for the angular momentum transfer process in the parity-unfavored transition of krypton atoms.

Experimentally, we obtained the fundamental laser pulses (800 nm, 25 fs, and p polarization) from a multipass Ti:sapphire laser amplifier operating at 3 kHz. We produced the second harmonic (400 nm, 35 fs, and s polarization) via frequency doubling using a 200-μm-thick β-barium borate crystal, and then the two light beams were arranged in a Mach-Zehnder interferometer [26,27]. In each arm of the interferometer, we guided the light beam through a $\lambda/2$ wave plate and a thin-film polarizer to control its polarization direction and intensity independently. Then the two light pulses recombined and the phase delay between the two colors was finely tuned by a pair of fused silica wedges with a tilt angle of 2°. The two-color fields were focused into a skimmed supersonic jet of krypton gas by a silver mirror in the reaction chamber. The intensity of the 400-nm light was calibrated at $\sim 3.2 \times 10^{13}$ W/cm^2 from the locations of above-threshold ionization (ATI) peaks, and the intensity of the 800-nm light was controlled at a perturbative weak level about 6.0×10^{11} W/cm^2, which was calibrated by the comparing results with those from the solution of the time-dependent Schrödinger equation (TDSE). We measured three-dimensional momenta of photoelectrons using cold target recoil ion momentum spectroscopy [28,29]. The static electric ($\sim$3.2 V/cm) and magnetic ($\sim$5.4-G) fields were applied in the spectrometer.

In Fig. 1(b), we illustrate the measured photoelectron momentum distribution in the single 400-nm light field. There are two sets of ATI structures corresponding to the two ionic states of $J_i = 1/2$ and $J_i = 3/2$ of Kr atoms, respectively. The first-order ATI from $J_i = 1/2$ shows a typical angular distribution of the parity-unfavored transition, i.e., the electron yield along the perpendicular direction is dominant. This angular distribution indicates that the states with nonzero m are populated, which is not allowed by the selection rule in the linearly polarized light. Using an experiment of continuously varying the light intensity (not shown), we have revealed that the parity-unfavored transition is assisted by a Freeman resonance with the intermediate $5p$ state [30]. The electron at the $5p$ state transits upwards to a weak-binding d_0 state after absorbing one photon. Then, the spin-orbit excited ion relaxes to its ground state (i.e., from $J_i = 1/2$ to $J_i = 3/2$), accompanying a transverse angular momentum transfer with the emitting electron. The electron population mostly transits from the d_0 state to d_1 and d_2 states correspondingly. Finally, the electron wave packet in the superposition state of d_0, d_1, and d_2 creates the parity-unfavored photoelectron structure. Using the least-squares fitting, one can estimate that the electron populations in the d_0, d_1, and d_2 states on the ATI are 24.9%, 7.8%, and 67.3%, respectively, as illustrated in Fig. 1(c).

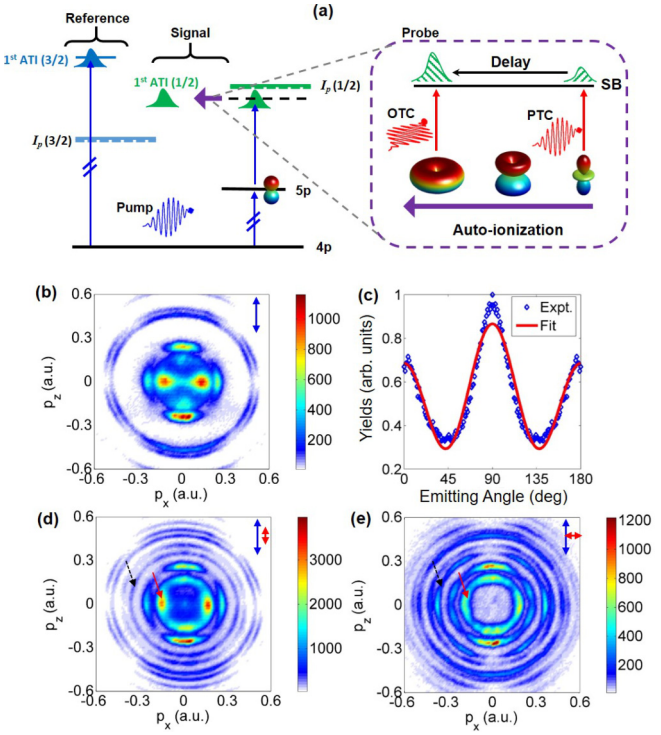

FIG. 1. Angular momentum transfer in the parity-unfavored photoionization of krypton atoms and the phase measurement with two-color fields. (a) Principle of measurement. When a krypton atom is ionized by a strong linearly polarized 400-nm light field (the pump), the first-order ATI from the channel of the $J_i = 1/2$ ionic state is formed by the resonance-assisted parity-unfavored transition where the electron angular momentum is transferred from d_0 to d_1 and d_2. A parallel (or orthogonal) 800-nm light field is used to probe the phase of the electron wave packet populated at the d_0 (or d_2) state. The electron wave packet from the $J_i = 3/2$ ionic state serves as the phase reference, allowing one to calibrate the measured phase from the $J_i = 1/2$ channel. (b) Measured photoelectron momentum distribution in the pump light field polarized along the z axis. There are two sets of ATI structures, corresponding to the two ionic states. The one with a lower energy is contributed from the $J_i = 1/2$ ionic state. (c) Photoelectron angular distribution of the first-order ATI from the $J_i = 1/2$ ionic state and its least-squares fitting with the d_0, d_1, and d_2 waves. The fitting result is $0.249Y_{20}(\theta)^2 + 0.078Y_{21}(\theta)^2 + 0.673Y_{22}(\theta)^2$, where $Y_{lm}(\theta)$ is the spherical harmonics and the photoelectron emitting angle is defined as $\theta = \arctan(p_x/p_z)$. As to the experimental curve, we integrated the photoelectron energy in the range of [0.2, 0.6] eV and performed the symmetrical operation in order to implement the fitting. (d) and (e) Phase-integrated photoelectron momentum distributions probed by a weak parallel (d) and orthogonal (e) linearly polarized 800-nm light fields. The blue and red arrows at the top-right corner mark the polarization directions of the 400-nm and 800-nm lights, respectively. The solid and dashed arrows mark the first-order ATI and the first-order sideband from $J_i = 1/2$, respectively. In (b), (d), and (e), the photoelectron momentum p_y along the light propagation direction was integrated in the range of $[-0.2, 0.2]$ eV.

Our goal is to measure the duration time of the angular momentum transfer. For this purpose, we use another weak linearly polarized 800-nm light field to probe the phases of the different-m components of the wave packet as shown in

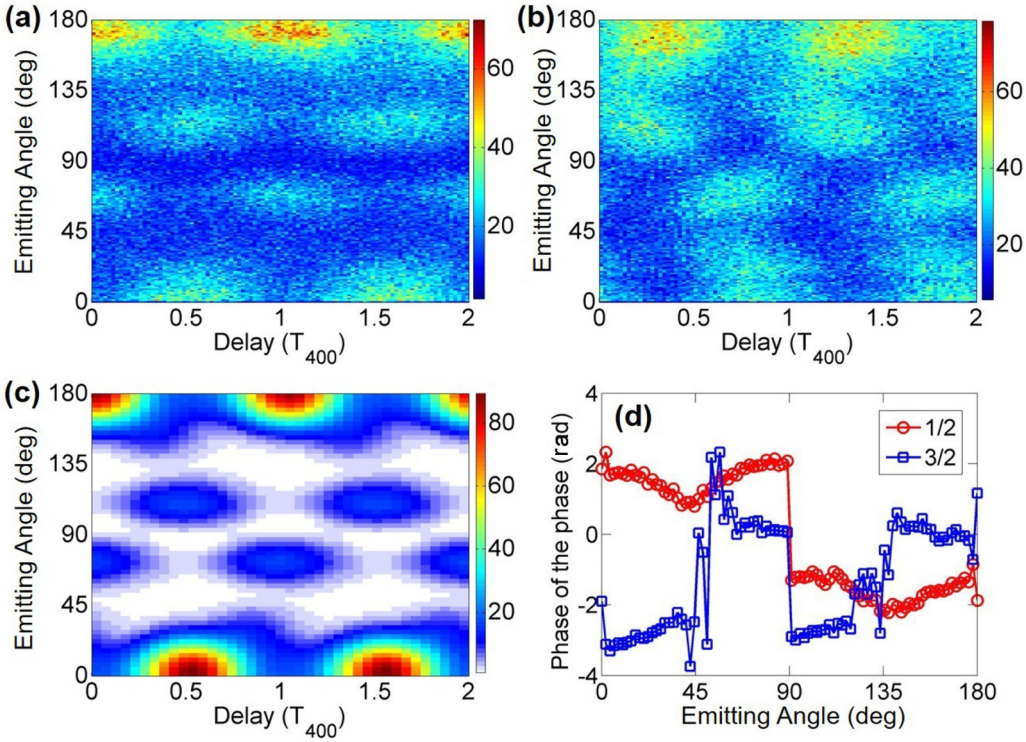

FIG. 2. Time-resolved angular distribution of the first-order sideband in the PTC fields. (a) and (b) Measured time-resolved photoelectron angular distributions from the (a) $J_i = 3/2$ and (b) $J_i = 1/2$ ionic states as a function of the phase delay between the two pulses. The photoelectrons are integrated in the energy range of [2.1, 2.7] eV for (a) and [1.4, 2.0] eV for (b). (c) Simulated time-resolved angular distribution of the $J_i = 3/2$ ionic state with the TDSE method. (d) Angle-resolved PP extracted from (a) and (b) using the Fourier transform.

Fig. 1(a). According to the shape of the electron orbitals and the polarization direction of the probe light, one can infer that the parallel (or orthogonal) probe light will selectively ionize the component in the d_0 (or d_2) state. Thus, one is able to extract the phase difference between the electron components in those two states, which is directly related to the duration time of the angular momentum transfer process since the d_0 state is mainly triggered before the process and the d_2 state can only be triggered after that. Therefore, the measurements with the PTC and the OTC fields, respectively, serve as the start and the stop of a stopwatch in our timing experiment.

In Figs. 1(d) and 1(e), we illustrate the measured phase-integrated photoelectron momentum distributions in the PTC and OTC fields, respectively. In the PTC fields, the crosswise electron yield on the first-order ATI from $J_i = 1/2$ is still dominant after the depletion by the ATI-to-sideband transition [see the red solid arrow in Fig. 1(d)], indicating that the d_2 component is less probed by this light. By contrast, in the OTC fields the crosswise electron yield on the ATI is reduced significantly [see the red solid arrow in Fig. 1(e)]. And the relative yield of the resulting sideband in the OTC fields is obviously larger than that in the PTC fields [see the black dashed arrows in Figs. 1(d) and 1(e)]. These observations validate that the light with a specific polarization can selectively probe the specific electron orbital.

As the same as the RABBIT, the phase of the probed electron wave is encoded in the phase of the sideband spectrum with respect to the two-color phase delay, i.e., phase of the phase (PP) [31], which is usually obtained by a sine fit or the Fourier transform. Generally, the time-delay τ converted from the PP (by dividing 2ω, ω is the frequency of the 800-nm field) can be decomposed as the sum of the contributions that reflect the steps of the sideband generation,

$$\tau = \tau_{\text{light}} + \tau_{\text{pump}} + \tau_{\text{res}} + \tau_{\text{put}} + \tau_{\text{cc}}, \tag{1}$$

in which τ_{light} is the group delay of the pump light, τ_{pump} is the accumulated time delay during the multiphoton ionization by the pump light, and τ_{cc} is the delay of the continuum-continuum transition from ATI to sideband in the probe process. Finally, τ_{res} is the delay of the resonance with the $5p$ state and τ_{put} is the delay of the parity-unfavored transition after the resonance, which are both peculiar to the channel of $J_i = 1/2$. Note that the sum of τ_{light}, τ_{pump}, and τ_{cc} is nearly common for the two ionic states of krypton [25], and, thus, we use the time delay obtained from $J_i = 3/2$ to calibrate the absolute delay of the parity-unfavored emission of $J_i = 1/2$. The phase difference between the two ionic states $\Delta\tau^{1/2-3/2} = \tau_{\text{res}} + \tau_{\text{put}}$ naturally eliminates τ_{light}, τ_{pump}, and τ_{cc}. The physical quantity of interest (i.e., τ_{put}) can, thus, be obtained.

In Figs. 2(a) and 2(b), we illustrate the measured angular distributions of the sidebands as a function of the two-color phase delay in the PTC fields from $J_i = 3/2$ and $J_i = 1/2$ ionic states, respectively. We use the Fourier transform to extract the PPs of the two sideband spectra as shown in Fig. 2(d). From the results, it is clear that the oscillations of the electrons from the two ionic channels are nearly out of phase, and their phase difference is larger than $\pi/2$ for most emission angles. Since the electron dynamics in the channel of $J_i = 3/2$ is ordinary, we can solve the TDSE within the single-active-electron

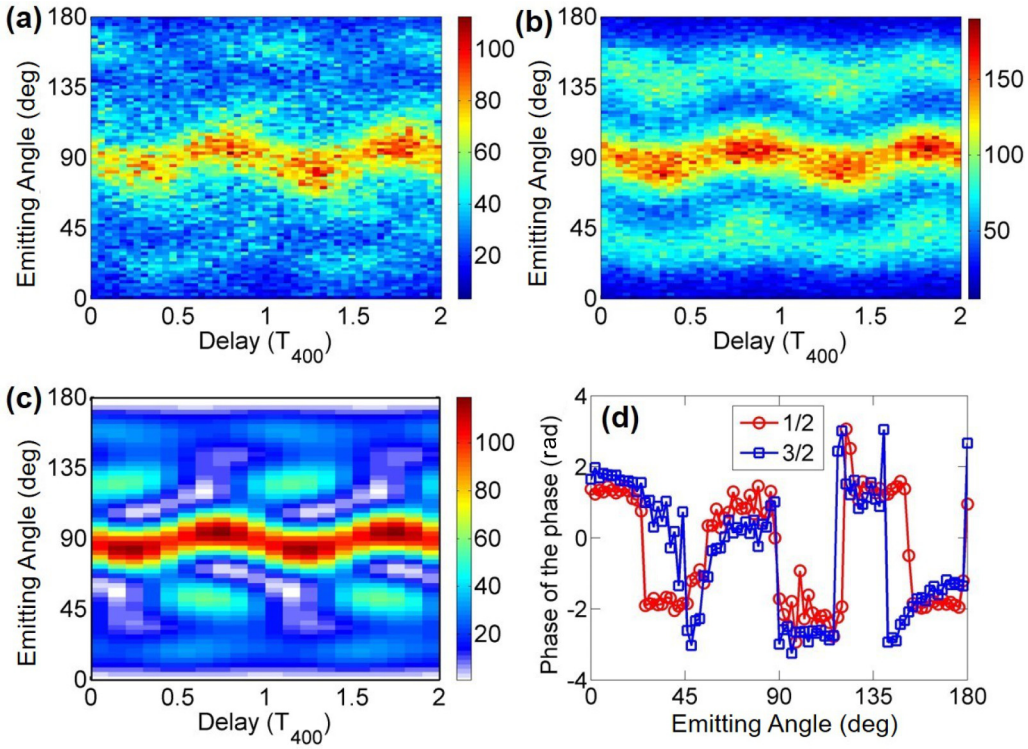

FIG. 3. Time-resolved results of the first-order sideband in the OTC fields. Figure captions are the same as those in Fig. 2.

approximation to calculate the corresponding time-resolved angular distribution [see Fig. 2(c)]. In the modeling [32], we used a model potential $V(r) = -\frac{1}{r} - \frac{A\ \exp(-Br)+(35-A)\exp(-Cr)}{r}$ with $A = 5.250$, $B = 0.902$, and $C = 3.640$ to simulate the ground $4p$ state of krypton ($I_p = 14.0$eV for $J_i = 3/2$) [33], and a $\sin^2$-envelope laser pulse with a duration of 12 400-nm cycles. The simulated spectrum agrees well with the experimental result. We have also checked electron populations at intermediate states in our simulation and validated that there is no resonance. Note that in our experiments the two-color phase delay is calibrated by the TDSE simulation of $J_i = 3/2$. Therefore, the channel of $J_i = 3/2$ can serve as a well-defined reference. In the PTC fields only the electron component at the d_0 state is probed and hence the measured phase shift of $J_i = 1/2$ with respect to $J_i = 3/2$ originates from the resonance in the channel of $J_i = 1/2$, i.e., $\Delta\tau_{\rm PTC}^{1/2-3/2} = \tau_{\rm res}$.

The corresponding results measured with the OTC fields are illustrated in Fig. 3. Owing to the polarization direction of the probe light, most electrons in the sideband are emitted along the angle of 90°. The TDSE simulation agrees well with our experimental result of $J_i = 3/2$, except the fact that the electron lobe ranging in 50°∼60° is more distinct in the calculation. When carefully comparing the extracted PPs from the two ionic states [see Fig. 3(d)], one can observe that there is only a tiny phase difference between the two channels for the lobe near 90°, which is in contrast with the PTC case. In this OTC case, the time delay of resonance is partially offset by the delay of the angular momentum transfer of the parity-unfavored transition, i.e., $\Delta\tau_{\rm OTC}^{1/2-3/2} = \tau_{\rm res} + \tau_{\rm put}$.

After subtracting the extracted PP of $J_i = 3/2$ from that of $J_i = 1/2$, we obtain the phase difference between the two ionic states as shown in Fig. 4(a). The phase difference is angle dependent due to the interference with different-l electron orbitals [34], and, thus, it is necessary to select some specific angles to convert the phase difference to the time delay of interest. In the PTC fields, we choose the emitting angle around 0°, i.e., the parallel-polarization direction of the two pulses since the electron components populated in the d_1 and d_2 states have no influence in this direction. Thus, the time delay of the parity-unfavored transition ($\tau_{\rm put}$) is not involved along this direction. The converted resonance time delay ($\tau_{\rm res}$) is 315 ± 32 as. In the OTC case, we focus on the phase difference along the angle of 90°, which corresponds to the polarization direction of the probe light and the orientation direction of the d_2 orbital as well. Thus, the contribution from the d_0 orbital is the least along this direction. Then the sum of $\tau_{\rm res}$ and $\tau_{\rm put}$ is retrieved, as illustrated in Fig. 4(b). Finally, after a differential procedure the time-delay $\tau_{\rm put}$ is measured to be -255 ± 81 as in Ref. [35]. The negative sign means that it is opposite to the resonance delay. Note that the positive resonance delay represents the resonance electron will be advanced when comparing with the free electron. So the negative time delay of the parity-unfavored transition is reasonable since the electron will be delayed due to the angular momentum transfer in the transition.

The Freeman resonance with the $5p$ state allows the electron to be populated to the levels between the $J_i = 3/2$ and the $J_i = 1/2$ thresholds, which is the prerequisite for the parity-unfavored channel. Because of the intensity averaging effect in the laser focus, the Freeman resonance can be observed in a large range of the light peak intensity, and, thus, this parity-unfavored channel is not very sensitive with

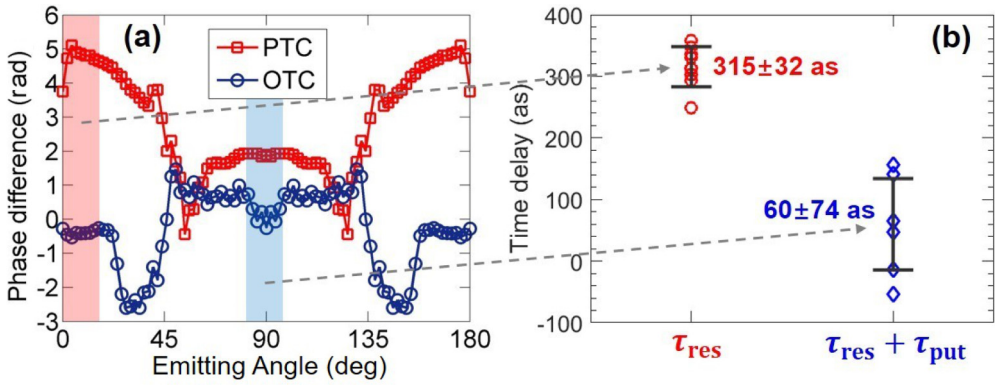

FIG. 4. (a) Phase difference between extracted PPs from the two ionic states. (b) Time delay from the resonance (τ_{res}), the sum of τ_{res}, and the time delay of the parity-unfavored transition (τ_{put}), which are converted from the phase difference at the emitting angle of 0° in the PTC fields and at the angle of 90° in the OTC fields, respectively. The integration window of the electron emitting angle is 10° as illustrated by the shadows in (a). In (b), the original data are marked with blue diamonds and red circles, and the mean value and the standard deviation are represented by the black error bars.

the intensity of the 400-nm light. In the Supplemental Material [36], we show the experimental results at a higher light intensity, i.e., 5.2×10^{13} W/cm^2. There the parity-unfavored channel is still clearly resolved, and the relative time delay is similar.

To justify the rationality of the measured time delay, one can estimate the time of the angular momentum change from d_0 to d_2 using an intuitive classical rotor model. The electron rotational angle from the d_0 state to the d_2 state is about 90°, and in the process the electron acquires the transferred angular momenta of $\pm 2\hbar$ along the rotation axis from the excited ion [30]. Therefore, the duration of the electron rotation could be estimated as $\tau_{\text{put}}^{\text{classical}} = \Delta\theta/\Delta\omega = (\pi/2)/(2\omega_{400}) \sim 167$ as, which is close to the measurement.

In conclusion, we have measured the characteristic time of the angular momentum transfer in the parity-unfavored transition of krypton atoms triggered by an intense ultraviolet light field. The phases of the electron wave functions with different magnetic quantum numbers are probed via an angle-resolved RABBIT-type scheme and are calibrated with the phase reference of the ground ionic state. The probes with the parallel and orthogonal lights serve as the start and the stop of a timing stopwatch, respectively, which provides a general approach to time resolve the orbital-dependent electron dynamics. This study has implication to explore time delays of many-body dynamical processes caused by electron correlations beyond the single-active-electron approximation in the multiphoton ionization.

This work was supported by the NSFC (Grants No. 92050201, No. 11434002, No. 11774013, No. 11725416, and No. 11527901).

[1] U. Fano and D. Dill, Phys. Rev. A **6**, 185 (1972).
[2] D. Dill, Phys. Rev. A **6**, 160 (1972).
[3] D. Dill and U. Fano, Phys. Rev. Lett. **29**, 1203 (1972).
[4] D. Dill, Phys. Rev. A **7**, 1976 (1973).
[5] D. Dill, A. F. Starace, and S. T. Manson, Phys. Rev. A **11**, 1596 (1975).
[6] U. Fano and C. H. Greene, Phys. Rev. A **22**, 1760 (1980).
[7] Chris H. Greene, Phys. Rev. Lett. **44**, 869 (1980).
[8] B. Langer, J. Viefhaus, O. Hemmers, A. Menzel, R. Wehlitz, and U. Becker, Phys. Rev. A **51**, R882 (1995).
[9] A. A. Wills, T. W. Gorczyca, N. Berrah, B. Langer, Z. Felfli, E. Kukk, J. D. Bozek, O. Nayandin, and M. Alshehri, Phys. Rev. Lett. **80**, 5085 (1998).
[10] P. M. Kraus and H. J. Wörner, Angew. Chem., Int. Ed. **57**, 5528 (2018).
[11] M. Mitrano, A. Cantaluppi, D. Nicoletti, S. Kaiser, A. Perucchi, S. Lupi, P. Di Pietro, D. Pontiroli, M. Riccò, S. R. Clark, D. Jaksch, and A. Cavalleri, Nature (London), **530**, 461 (2016).
[12] P. M. Paul, E. S. Toma, P. Breger, G. Mullot, F. Augé, P. Balcou, H. G. Mulller, and P. Agostini, Science **292**, 1689 (2001).
[13] M. Hentschel, R. Kienberger, C. Spielmann, G. A. Reider, N. Milosevic, T. Brabec, P. Corkum, U. Heinzmann, M. Drescher, and F. Krausz, Nature (London) **414**, 509 (2001).
[14] M. Drescher, M. Hentschel, R. Kienberger, M. Uiberacker, V. Yakovlev, A. Scrinzi, T. Westerwalbesloh, U. Kleineberg, U. Heinzmann, and F. Krausz, Nature (Lonndon) **419**, 803 (2002).
[15] M. Schultze *et al.*, Science **328**, 1658 (2010).
[16] K. Klünder *et al.*, Phys. Rev. Lett. **106**, 143002 (2011).
[17] M. Huppert, I. Jordan, D. Baykusheva, A. von Conta, and H. J. Wörner, Phys. Rev. Lett. **117**, 093001 (2016).
[18] A. L. Cavalieri *et al.*, Nature (London) **449**, 1029 (2007).
[19] J. Itatani, F. Quéré, G. L. Yudin, M. Y. Ivanov, F. Krausz, and P. B. Corkum, Phys. Rev. Lett. **88**, 173903 (2002).
[20] H. G. Muller, Appl. Phys. B: Lasers Opt. **74**, s17 (2002).
[21] L. J. Zipp, A. Natan, and P. H. Bucksbaum, Optica **1**, 361 (2014).
[22] M. Richter, M. Kunitski, M. Schöffler, T. Jahnke, L. P.H. Schmidt, M. Li, Y. Liu, and R. Dörner, Phys. Rev. Lett. **114**, 143001 (2015).
[23] S. Beaulieu *et al.*, Science **358**, 1288 (2017).
[24] P. Ge, M. Han, M.-M Liu, Q. Gong, and Y. Liu, Phys. Rev. A **98**, 013409 (2018).
[25] I. Jordan, M. Huppert, S. Pabst, A. S. Kheifets, D. Baykusheva, and H. J. Wörner, Phys. Rev. A **95**, 013404 (2017).
[26] M. Han, P. Ge, Y. Shao, M.-M. Liu, Y. Deng, C. Wu, Q. Gong, and Y. Liu, Phys. Rev. Lett. **119**, 073201 (2017).

[27] M. Han, P. Ge, Y. Shao, Q. Gong, and Y. Liu, Phys. Rev. Lett. **120**, 073202 (2018).

[28] R. Dörner, V. Mergel, O. Jagutzki, L. Spielberger, J. Ullrich, R. Moshammer, and H. Schmidt-Böcking, Phys. Rep. **330**, 95 (2000).

[29] J. Ullrich, R. Moshammer, A. Dorn, R. Dorner, L. P. H. Schmidt, and H. Schmidt Bocking, Rep. Prog. Phys. **66**, 1463 (2003).

[30] M. Han, P. Ge, Y. Fang, X. Yu, Z. Guo, Y. Deng, C. Wu, Q. Gong, and Y. Liu, Phys. Rev. A **101**, 061401(R) (2020).

[31] S. Skruszewicz, J. Tiggesbäumker, K.-H. Meiwes-Broer, M. Arbeiter, T. Fennel, and D. Bauer, Phys. Rev. Lett. **115**, 043001 (2015).

[32] L.-Y. Peng and Q. Gong, Comput. Phys. Commun. **181**, 2098 (2010).

[33] F. Cloux, B. Fabre, and B. Pons, Phys. Rev. A **91**, 023415 (2015).

[34] D. Busto, J. Vinbladh, S. Zhong, M. Isinger, S. Nandi, S. Maclot, P. Johnsson, M. Gisselbrecht, A. L'Huillier, E. Lindroth, and J. M. Dahlström, Phys. Rev. Lett. **123**, 133201 (2019).

[35] The uncertainty of τ is calculated by $\sigma_{\text{put}} = \sqrt{\sigma_{\text{res}}^2 + \sigma_{\text{sum}}^2}$, where σ_{res} and σ_{sum} are the measured uncertainties of τ_{res} and the sum of τ_{put} and τ_{res}, respectively. Due the periodicity of the retrieved phase, strictly speaking there is $\tau_{\text{put}} = (-255 \pm 81)$ as $+ nT_{400}$, where n is an integer. The parity-unfavored electron transition is an ultrafast attosecond process, and, thus, we select -255 ± 81 as as the final result.

[36] See Supplemental Material at http://link.aps.org/supplemental/10.1103/PhysRevA.102.061101 for the experimental results at the intensity of 5.2×10^{13} W/cm^2 for the 400-nm light.